



# Photosynthetic microorganisms coupled photodynamic therapy for enhanced antitumor immune effect

Haoran Wang<sup>a,c,1</sup>, Honghui Liu<sup>a,1</sup>, Yunfei Guo<sup>a</sup>, Wenjing Zai<sup>a</sup>, Xianghui Li<sup>a</sup>, Wei Xiong<sup>b</sup>, Xiaozhi Zhao<sup>e</sup>, Yingfang Yao<sup>b</sup>, Yiqiao Hu<sup>a,d</sup>, Zhigang Zou<sup>b,d</sup>, Jinhui Wu<sup>a,d,\*</sup>

<sup>a</sup> State Key Laboratory of Pharmaceutical Biotechnology, Chemistry and Biomedicine Innovation Center, Medical School and School of Life Sciences, Nanjing University, Nanjing, 210093, China

<sup>b</sup> National Laboratory of Solid State Microstructures, Collaborative Innovation Center of Advanced Microstructures, School of Physics, Nanjing University, Nanjing, 210093, China

<sup>c</sup> School of Basic Medical Science, Nanjing University of Chinese Medicine, Nanjing, China

<sup>d</sup> Jiangsu Key Laboratory for Nano Technology, Nanjing University, Nanjing, 210093, China

<sup>e</sup> Department of Urology, Drum Tower Hospital, Medical School, Nanjing University, Nanjing, 210093, China

## ARTICLE INFO

### Keywords:

*Chlorella*  
Photodynamic therapy  
Controlled adjuvants release  
Systemic antitumor immune response  
Immune memory effect

## ABSTRACT

The ideal photodynamic therapy (PDT) should effectively remove the primary tumor, and produce a stronger immune memory effect to inhibit the tumor recurrence and tumor metastasis. However, limited by the hypoxic and immunosuppressive microenvironment, the PDT efficiency is apparently low. Here, *Chlorella (Chl.)* is exploited to enhance local effect by producing oxygen to reverse hypoxia, and release adjuvants to reverse immunosuppressive microenvironment to enhance abscopal effect afterwards. Results from different animal models indicated that *Chl.* could enhance local effect and PDT related immune response. Ultimately, *Chl.* coupled PDT elicited anti-tumor effects toward established primary tumors (inhibition rate: 90%) and abscopal tumors (75%), controlled the challenged tumors (100%) and alleviated metastatic tumors (90%). This *Chl.* coupled PDT strategy can also produce a stronger anti-tumor immune memory effect. Overall, this *Chl.* coupled PDT strategy generates enhanced local tumor killing, boosts PDT-induced immune responses and promotes anti-tumor immune memory effect, which may be a great progress for realizing systemic effect of PDT.

## 1. Introduction

Developing effective anti-tumor therapies are urgently needed to eradicate solid tumors, as well as disseminated and undetectable metastatic tumor cells, and can further prevent tumor recurrence [1–3]. Photodynamic therapy (PDT) has been widely studied as a promising strategy for primary solid tumors [4–6]. In PDT, laser irradiation is used to transfer molecule oxygen into reactive oxygen species (ROS) for tumor killing [7,8]. However, tumor hypoxia will strongly limit the local therapeutic effect of PDT. Current studies related PDT on tumor hypoxia reversal mainly focus on the strategies how to deliver oxygen to PDT for achieving better local effect, including physical and chemical oxygen supply [9–11]. Physical oxygen supply is achieved by dissolving O<sub>2</sub> in a

high-oxygen-solubility medium such as perfluorocarbon (PFC) [12–14]. Chemical oxygen supply is achieved by chemical reaction between enzymes or chemical molecules and overexpressed factors in tumors [15–17]. These oxygen delivery strategies yet have made a great improvement on local effects of PDT even though the oxygen capacity is limited [18,19].

Recently, PDT has been reported to have the capacity to elicit adaptive anti-tumor immune response since a large number of tumor-associated antigens (TAAs) can be released post PDT to trigger dendritic cells (DCs) and activate cytotoxic T lymphocytes (CTLs), which help PDT shift from local effects to systemic effects [20–25]. This systemic effects displayed by PDT show a great potential in the treatment of patient with tumor metastasis and tumor recurrence [24,26,27].

Peer review under responsibility of KeAi Communications Co., Ltd.

\* Corresponding author. State Key Laboratory of Pharmaceutical Biotechnology, Chemistry and Biomedicine Innovation Center, Medical School, Nanjing University, Nanjing, 210093, China.

E-mail address: [wuj@nju.edu.cn](mailto:wuj@nju.edu.cn) (J. Wu).

<sup>1</sup> These authors contribute equally.

<https://doi.org/10.1016/j.bioactmat.2021.10.028>

Received 25 August 2021; Received in revised form 18 October 2021; Accepted 18 October 2021

Available online 28 October 2021

2452-199X/© 2021 The Authors. Publishing services by Elsevier B.V. on behalf of KeAi Communications Co. Ltd. This is an open access article under the CC

BY-NC-ND license (<http://creativecommons.org/licenses/by-nc-nd/4.0/>).

However, exacerbated immunosuppressive environment will obviously inhibit the incidence of systemic effect of PDT. This is also the reason that local effects by PDT often results in tumor recurrence and limits its wide use in clinic [28]. Boosting adaptive immunity post PDT by continuously supplying adjuvants pool is a potential effective strategy for completely eradicating metastatic tumor cells and tumor recurrence.

Due to the natural advantages, microorganisms have been coupled with standard tumor therapies, and they have achieved improved efficacy [29–31]. Photosynthetic microorganisms (PSMs), such as *Chlorella* (*Chl.*), have long been recognized as the origin of oxygen in Earth's atmosphere [32,33]. *Chl.* can continuously produce oxygen until the light exposure is removed [34], which might be an unlimited oxygen source for PDT. Meanwhile, *Chl.* has been widely reported to release immunostimulatory substances after digestion [35–37], such as abundant  $\beta$ -glucan and mannan, which have been identified for recruiting antigen-presenting cells (APCs) [38]. In addition, *Chl.* eventually forms an adjuvants pool after being destroyed, including the extracts (hot-water-soluble polysaccharides from *Chl.*, CWST) and the water-soluble glycoproteins (ARS-2 and so on), which has an effect on activating DCs and macrophages through toll-like receptor (TLR) [35,39]. And *Chl.* have extremely low immunogenicity and adjuvants effect when remaining intact, they can only perform adjuvants effect when they were not integrated.

Here, we developed a *Chl.* coupled PDT that utilizing the oxygen production ability and adjuvants releasing ability of *Chl.* to enhance PDT on local tumor and strengthen PDT-induced systemic anti-tumor immune response (Fig. 1). *Chl.* is exploited to enhance local effect by producing oxygen to reverse hypoxia and to generate more ROS under the action of irradiated photosensitizer (PS), eventually exposing more TAAs. Besides, the released adjuvants (ARS-2 and etc.) by *Chl.* further reverse immunosuppressive microenvironment and increase the activation of DCs through toll-like receptor 2 (TLR2) and etc. Mature DCs will move to the lymph nodes and eventually activate CD8<sup>+</sup> cytotoxic T lymphocytes (CTLs) to produce adaptive immune response against specific tumor cells and enhance abscopal anti-tumor effect afterwards. The adjuvant releasing process is initiated during the PDT process. Hence, *Chl.* performs dual effects during the whole PDT process, including oxygen generation and adjuvants release. Ultimately, *Chl.*

coupled PDT can generate enhanced local tumor killing, boosts PDT induced immune responses and promotes immune memory effect, which may be a great progress for realizing systemic effect of PDT.

## 2. Materials and methods

**Materials.** HSA solution was purchased from Octapharma. Ce6 was obtained from Aladdin Industrial Corporation. The perfluorotributylamine (PFTBA) was supplied by Merger Chemical Technology Co. Ltd. (Shanghai, China). Roswell Park Memorial Institute 1640 (RPMI 1640), fetal bovine serum (FBS), Trypsin-EDTA and penicillin were purchased from Gibco (Thermo fisher, US). Dimethyl sulfoxide (DMSO) and ethanol were obtained from Sinopharm Chemical Reagent Co. HIF-1 $\alpha$  antibody, pimonidazole and its antibody were provided by Sigma-Aldrich Chemical Corporation. Cell counting kit 8 was supplied by Dojindo Laboratories (Japan). Singlet Oxygen Sensor Green (SOSG) and carbon-H<sub>2</sub>DCFDA were obtained from Molecular Probes Inc. DAPI and Micro NO Content Assay Kit were supplied by Keygen BioTech. Anti-CD11c antibody, anti-CD3 antibody, anti-CD4 antibody, anti-CD8 antibody, anti-CD86 antibody, anti-CD80 antibody anti-CD11b antibody, anti-F4/80 antibody, anti-CD44 antibody and anti-CD62L antibody were purchased from Proteintech. CT-26 cells, A549 cells and 4T1 cells were obtained from the Cell Bank of Shanghai Institutes for Biological Sciences, Chinese Academy of Sciences (Shanghai, China). Balb/c and Balb/c-nu mice were purchased from Yangzhou University Medical Center (Yangzhou, China). All other reagents were obtained from Sigma-Aldrich. *Chlorella* was donated by Kunshan Innovation Institute of Nanjing University.

***Chlorella* culture, count and collection.** *Chlorella* was cultured in BG-11 medium at 28 °C. The pH of BG-11 medium was maintained between 7.2 and 7.8.5% CO<sub>2</sub> was supplied to the illumination incubator. Light irradiation of 2500–3500 lux was administered in a 10/10 (day/night) cycle. Before the experiments, *Chlorella* was centrifuged at 5500 rpm for 5 min. Then the *Chlorella* was rinsed three times with 0.9% normal saline (NS). And then, the *Chlorella* was resuspended by BG-11 or RPMI 1640 to  $4 \times 10^7$  cfu/ml or  $3 \times 10^8$  cfu/ml. The number of the *Chlorella* was determined by the optical density (OD) at 683 nm. The quantitative relation between the OD<sub>683</sub> and the number of the *Chlorella*

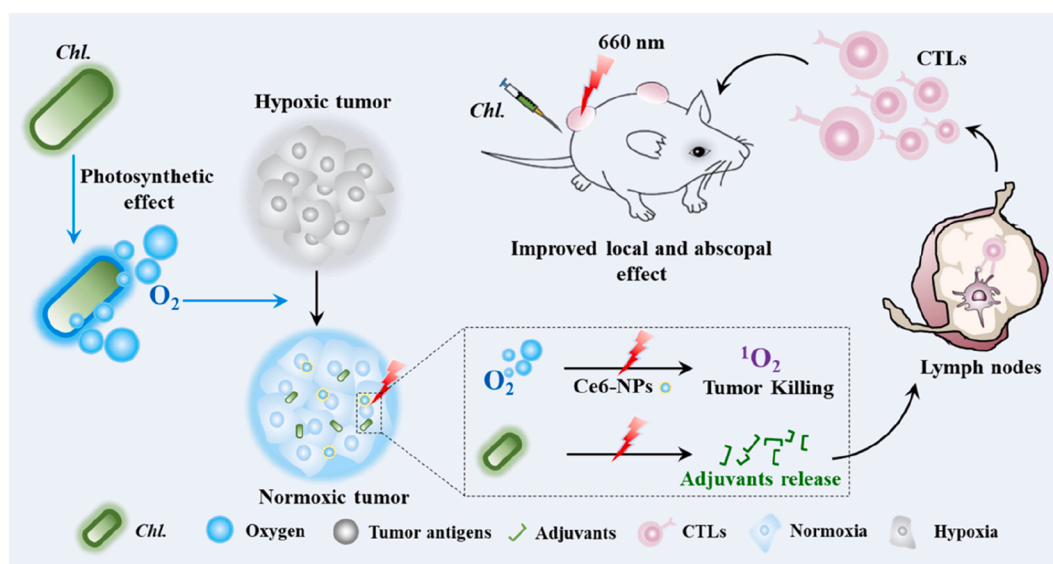


**Fig. 1. Schematic diagram of the *Chl.* coupled PDT strategy for enhanced local and abscopal anti-tumor effects.** *Chl.* were firstly injected into mice and then irradiated with laser illumination. *Chl.* can be taken as oxygen suppliers to produce O<sub>2</sub> under laser illumination which can reverse tumor hypoxia environment, strengthen Ce6-NPs based PDT against tumor and produce tumor associated antigen for further immune activation. Immunoactive substances released by *Chl.* post PDT can be taken as immune adjuvants, which increase the activation of dendritic cells (DCs) and promote the production of anti-tumor cytotoxic T lymphocytes (CTLs). *Chl.* coupled PDT enhanced PDT-related immune responses and elicited anti-tumor effects toward abscopal tumors (75%), controlled the challenged tumors (100%) and alleviated metastatic tumors (90%).

was determined by counting the hemocytometer. The morphology of *Chlorella* was observed using an optical microscope. Meanwhile *Chlorella* was measured by the O<sub>2</sub> microelectrode to test the vitality.

**Cell line and tumor models on mice.** RAW 264.7 cells were cultured in DMEM medium supplemented with 10% fetal bovine serum and 1% L-glutamine (200 mM). CT26 cells were cultured in RPMI 1640 medium supplemented with 10% fetal bovine serum and 1% L-glutamine (200 mM). A549 cells were cultured in DMEM medium supplemented with 10% fetal bovine serum and 1% L-glutamine (200 mM). 4T1 cells were cultured in DMEM medium supplemented with 10% fetal bovine serum and 1% L-glutamine (200 mM). Passaging the CT26, A549 and 4T1 cells when the confluence of the cells came to 60–80%. Balb/c and Balb/c-nu mice were raised in a group of six to ten with free access to abundant food and water. To establish CT26, 4T1 and A549 tumor models, fur of the Balb/c and Balb/c-nu mice was carefully removed.  $1 \times 10^6$  CT26, A549 and 4T1 cells of 0.05 ml were then injected subcutaneously into the outer flank of the mouse. When the tumor volume reached approximately 100–150 mm<sup>3</sup>, the experiments were conducted on these mice.

Animals were observed daily for any clinically relevant abnormalities during the study period. If any of the mice was moribund due to therapeutic toxicity, severe ulceration around the subcutaneous tumor appeared in mice or the body weight of the mice decreased by 20% compared with the pre-study, mice were euthanized. All animal tests and experiment procedures used in this experiment were performed in accordance with protocols approved by the Institutional Animal Care and Use Committee of Nanjing University (NJU-IACUC, IACUC2003160).

**In vitro oxygen production of the *Chlorella* (*Chl.*).** To compare the viability and to demonstrate the photosynthetic action of the *Chl.*, oxygen production was needed to be valued. 3 mL  $4 \times 10^7$  cfu/ml *Chlorella* solution was prepared and irradiated by the red light (~600 nm) (wavelength: 590–700 nm, 150 W) at 10,000 lux. The oxygen concentration of the solution was measured every 3 s using an oxygen probe (OX-NP, 1.6 × 40 mm-needle sensor for piercing, Unisense A/S CO. LTD). To check if the *Chlorella* could continue to product oxygen, repeated cycles of light were given. The buffer outside of the *Chlorella* was changed to be hypoxia one after each cycle.

**Alleviation of Cellular Hypoxia in vitro.** The hypoxia alleviation ability of photosynthetic oxygen production in CT26 cells was investigated and the hyperoxia group was set as the positive one. Generally, CT26 cells were seeded into 24-well plates at a density of  $2.5 \times 10^4$  cells per well. After 24 h incubation, cells were placed under hypoxia incubator (1% O<sub>2</sub>) in the presence or absence of *Chlorella* ( $4 \times 10^7$  cfu/ml). One of the *Chlorella* groups was given light for 30min. After washed by PBS, the cells were evaluated by the protein HIF-1 $\alpha$  (hypoxia-inducible factor-1 $\alpha$ ). Antibody against HIF-1 $\alpha$  (Thermal Fisher Inc.) was used to evaluate the degree of hypoxia. Briefly, cells were incubated with rabbit anti-mouse labeled HIF-1 $\alpha$  antibody (dilution 1:800) at 37 °C for 1 h, followed by FITC labeled rat anti-rabbit IgG (dilution 1:800, Thermal Fisher Inc.) staining at 37 °C for 1 h. Tumor nucleus was stained by DAPI (4, 6-diamidino-2-phenylindole) for 5 min. Finally, fluorescence images of the cells were obtained by a fluorescence microscope (Nikon, Japan).

**In vivo hypoxia alleviation assessment.** To study the hypoxia reversal ability of the *Chlorella* in tumors, different endogenous or exogenous hypoxia marker Pimonidazole was used. For Pimonidazole based hypoxia detecting, CT26 tumor-bearing mice (150 mm<sup>3</sup>) were firstly injected with Pimonidazole hydrochloride (Hypoxyprobe Inc, USA) ( $60 \text{ mg kg}^{-1}$ ). 1 h later, the *Chlorella* ( $4 \times 10^7$  cfu/ml, 0.05 ml) was injected into the tumor and one of the groups was supplied with laser (660 nm, 170 mW/cm<sup>2</sup>) for 5 min. Then, the mice were sacrificed 30 min later to collect tumors. The tumors were embedded into OCT and were cut into 8  $\mu\text{m}$  slices. Tumor sections were then stained with FITC labeled rabbit-anti-mouse Pimonidazole antibody (dilution 1:200) at overnight 4 °C. Tumor nucleus then was stained by DAPI for 5 min. Finally, fluorescence images of the slices were observed by a fluorescence microscope (Nikon, Japan).

**Synthesis of Ce6@PFTBA@HSA nanoparticles (Ce6-NPs).** To prepare Ce6@ PFTBA @HSA nanoparticles, the method of unfolding/self-assembling method reported by our group previously was adopted. Briefly, HSA (90 mg) was mixed in deionized water (2.15 ml), stirring for 5 min. Then, 200  $\mu\text{l}$  of free Ce6 (1 mg/ml) dissolved in ethanol, 600 PFTBA  $\mu\text{l}$  was added to HSA solution, Ce6@ PFTBA @HSA nanoparticles were formed under at 300 W ultrasonic intensity in ice bath for 14 min. Free Ce6 was removed by ultrafiltration centrifuge tube (Millipore) for 10 min. According to standard curve of Ce6, the quantitation of Ce6 in Ce6@ PFTBA @HSA nanoparticles was determined by UV-vis absorption spectra (UV-2450, Shimadzu, Japan). By dynamic light scattering (DLS, 90 Plus, Brookhaven Instrum. Corp), the surface potential and the particle sizes of nanoparticles were measured. The structures of the sample were characterized by TEM (Tecan G<sup>2</sup> F20 S-Twin).

**Generation and detection of the <sup>1</sup>O<sub>2</sub> in vitro.** To detect the <sup>1</sup>O<sub>2</sub> production, a commercial single oxygen (<sup>1</sup>O<sub>2</sub>) specific dye, Singlet Oxygen Sensor Green (SOSG, Invitrogen Corp, USA) was used. Different samples of 100  $\mu\text{l}$  were added in 96-well (concentration of Ce6 is 10  $\mu\text{g}/\text{ml}$ , concentration of *Chlorella* is  $4 \times 10^7$  cfu/ml), then mixed with 20  $\mu\text{l}$  SOSG (50  $\mu\text{M}$ ). The <sup>1</sup>O<sub>2</sub> generation was qualified by multifunctional microplate reader (Ex/Em = 504/525 nm) after NIR (660 nm, 170 mW/cm<sup>2</sup>) irradiation at different time interval.

**Cytotoxicity experiments of Ce6-NPs in vitro.** CT26 cells were pre-seeded in 96-well plates at a density of 5,000 cells per well and incubated for 24 h Ce6-NPs of 0, 1, 2, 4, 8, 12, 16  $\mu\text{g}/\text{ml}$  (concentration of Ce6) were added into each well and incubated for 30min. After that, the cells were washed by PBS for twice. Different solutions (with *Chlorella* at the concentration of  $4 \times 10^7$  cfu/ml) which were prepared well in advance were added into the wells. The *Chl.* group was irradiated with ~600 nm red light (10000 lux, 150 W) for 30 min. All experiment groups were supplied with laser (660 nm, 170 mW/cm<sup>2</sup>) for 30 s. Then another 24 h of incubation was carried out. The cell viability was performed by the Cell Counting Kit-8 (CCK-8, DOJINDO). Cells treated by blank RPMI 1640 were set as control. Finally, the absorbance was measured at 450 nm using a microplate reader.

**Collection and characterization of supernatant protein of *Chl.* under 660 nm laser.** After adding Ce6 at 10  $\mu\text{g}/\text{ml}$  to *Chl.* ( $4 \times 10^7$  cfu/ml), Some groups were given photodynamic therapy, and some not. The laser (660 nm) was 170 mW and each group was irradiated for 30 s for 4 times. The supernatant was collected and centrifuged at 5500 rpm/min for 5 min, and the supernatant was collected later. Finally, the suspension was concentrated using a centrifugal concentrator (LABCONCO CentriVap), and the protein concentration was quantified using a BCA kit. We then applied the concentrated supernatant to SDS-PAGE. Corresponding bands were calibrated with a protein standard of 10–180 kDa (Marker: Solarbio, PR1910). Protein (maybe Glyco-protein) concentration was performed using SDS-PAGE and proteins that had just run into the separation gel were digested. Peptide mass spectrometry was then used for protein analysis.

**Immuno-activation characterization on BMDCs in vitro.** Balb/c mice (without any experiment) were executed and were soaked in 75% (v/v) alcohol. Isolated the mice's lower extremities and removed the muscle tissue of the extremities. Femurs and tibias were cut off and the cartilage of them were removed. Rinsing the bone marrow in the marrow cavity with a syringe containing DMEM supplemented with 15% FBS. The medium of the MSCs were changed totally after 6–8 h incubation. The MSCs were incubated with DMEM containing 20 ng/ml GM-CSF, 5% (v/v) FBS, 0.1% (w/v) 2-mercaptoethanol at the atmosphere of 37 °C, 5% CO<sub>2</sub>. When the cells grew to 80% confluence, cells were digested and were counted to a certain concentration.

The BMDCs were pre-seeded at a density of  $1 \times 10^5$  in 6-well plates and were incubated for 24 h. A certain amount of tumor antigens (tumor supernatant post PDT, 10  $\mu\text{g}/\text{ml}$ ), *Chl.* (post PDT, 3.3  $\mu\text{g}/\text{ml}$ ) acquired in advance and LPS (10  $\mu\text{g}/\text{ml}$ ) were incubated with the BMDCs for another 24 h. The *Chl.* culture supernatant were diluted with the same dilution factor and added. The concentration of intact *Chl.* was also 3.3  $\mu\text{g}/\text{ml}$ .

The cells were gathered and the supernatant of each well was collected. The cells were labeled with CD11c<sup>+</sup> antibody (FITC labeled), CD80<sup>+</sup> antibody (APC labeled) and CD86<sup>+</sup> antibody (PE labeled), cells were analyzed by flow cytometry (FACS-Calibur, BD Corp.). Data were obtained and analyzed using the FlowJo programs. The IL-12 and TNF- $\alpha$  of the supernatant were measured by mouse precoated ELISA kit (DAKEWE). Cells treated by blank PBS was set as control.

**Immuno-activation characterization on RAW 264.7 in vitro.** The RAW 264.7 cells were pre-seeded at a density of  $1 \times 10^5$  in 6-well plates and were incubated for 24 h. A certain amount of tumor antigens (tumor supernatant post PDT, 10  $\mu\text{g/ml}$ ), *Chl.* (post PDT, 3.3  $\mu\text{g/ml}$ ) acquired in advance and LPS (10  $\mu\text{g/ml}$ ) were incubated with the RAW 264.7 cells for another 24 h. The *Chl.* culture supernatant were diluted with the same dilution factor and added. The concentration of intact *Chl.* was also 3.3  $\mu\text{g/ml}$ . The cells were gathered and the supernatant of each well was collected. The cells were labeled with CD11b<sup>+</sup> antibody, CD45<sup>+</sup> antibody, F4/80<sup>+</sup> antibody, CD86<sup>+</sup> antibody, cells were analyzed by flow cytometry (FACS-Calibur, BD Corp.). Data were obtained and analyzed using the FlowJo programs. The IL-6 of the supernatant was measured by mouse precoated ELISA kit (DAKEWE). The NO of the supernatant was measured by NO kit (BIYUNTIAN). Cells treated by blank PBS was set as control.

**In vivo Chlorella enhanced PDT therapy of local tumor and absopal tumor.** Mice bearing CT26 tumors were randomly divide into two groups ( $n = 10$  of each group). Ce6-NPs (100  $\mu\text{g/ml}$ ) of 0.2 ml were directly injected into the corresponding group's mice intravenously. Time dependence of accumulation of Ce6-NPs was detected using small animal near-infrared imaging. After injection, the tumor regions were injected with the *Chl.*, which was given a  $\sim 600$  nm light for 30min. At a power density of  $1\text{W/cm}^2$ , the two NIR (660 nm) groups were given the laser at the tumor regions for 30s. The irradiation process contained two consecutive 15s applications with a 1-min interval. Tumor size was measured everyday using a vernier caliper after the treatment. The tumor volume was calculated according to the following equation: tumor volume = width  $\times$  width  $\times$  length/2. And the tumors were harvested at the last day. Parts of the tumors were preserved in 4% (w/v) paraformaldehyde and parts were embedded with OCT. Meanwhile body weights were monitored every day.

**Post-treatment dendritic cells infiltration in vivo.** Mice bearing CT26 tumors were randomly divide into four groups ( $n = 5$  each group). Experiment was taken as same as above. At the third day, the inguinal lymph nodes of the mice were harvested to be digested and to be collected. Then a certain number of cells were resuspended with PBS and anti-CD11c, anti-CD80 and anti-CD86 antibodies were added for 30min. Subsequently, the cells were washed once with PBS. The cells were then centrifuged, resuspended in 1 ml PBS. Then analyzed by flow cytometry (FACS-Calibur, BD Corp.). Data were obtained and analyzed using the FlowJo programs.

**Post-treatment T lymphocytes infiltration in vivo.** Mice bearing CT26 tumors were randomly divide into four groups ( $n = 5$  each group). Experiment was taken as same as above. At the 7th day, the tumors of the mice were harvested. Parts of the tumors were embedded into OCT and were cut into 8  $\mu\text{m}$  slices. Tumor slices were incubated with CD3<sup>+</sup>, CD4<sup>+</sup> and CD8<sup>+</sup> antibodies (dilution 1:800, Thermal Fisher Inc.) overnight at 4  $^\circ\text{C}$ . Tumor nucleus was stained by DAPI for 5min. Finally, fluorescence images of the slices were obtained by fluorescence microscope (Nikon, Japan). Meanwhile, a certain number of cells in the other part of the tumor were resuspended with PBS and anti-CD3, anti-CD4 and anti-CD8 antibodies were added for 30min. Subsequently, the cells were washed once with PBS. The cells were then centrifuged, resuspended in 1 ml PBS. Then analyzed by flow cytometry (FACS-Calibur, BD Corp.). Data were obtained and analyzed using the FlowJo programs.

**Data availability.** The authors declare that the main data supporting the findings of this study are available within the article and its Supplementary Information. Additional data are available from the corresponding author upon request.

### 3. Results

#### 3.1. Utilizing *Chl.* to enhance PDT based tumor cell killing in vitro

To verify that *Chl.* coupled PDT can effectively enhance the efficacy of photodynamic therapy *in vitro*, we conducted the following experiments. For that *Chl.* coupled PDT is composed by Ce6-NPs and *Chl.* (*Chl.*+Ce6-NPs+ $\sim 600$  nm + 660 nm) (Fig. 2a, Figure S1), we first prepared photosensitizer (PS) containing nanoparticles (Ce6-NPs) following our previous studies [40–44], and the diameter of the obtained Ce6-NPs is  $\approx 115$  nm (Figure S2). Meanwhile, we designed experiments to characterize the oxygen production capacity of *Chl.* The result showed that *Chl.* can efficiently produce oxygen under light irradiation (Fig. 2b), and still had the ability to produce sufficient oxygen after multiple irradiations (Fig. 2c). More importantly, the oxygen produced by *Chl.* can effectively reverse the tumors hypoxia *in vitro* (Figure S3). To detect whether the oxygen produced by *Chl.* can indeed be used by PSs during PDT and increase the PDT efficiency *in vitro*, we conducted experiments to test the enhanced PDT by oxygen produced by *Chl.* Using Singlet Oxygen Sensor Green (SOSG), we found that *Chl.* could greatly enhance the production of  $^1\text{O}_2$ , which was even higher than that in 95%  $\text{O}_2$  group (Fig. 2d). We then measured the amount of ROS in the cells using the commercial ROS probe  $\text{H}_2\text{DCFDA}$ . Results showed that *Chl.* coupled PDT had effectively increased the ROS production (Fig. 2e). At the same time, photodynamic cytotoxicity of *Chl.* coupled PDT group increased significantly (Fig. 2f) after Ce6-NPs were taken in by CT26 cells.

#### 3.2. Adjuvants released by *Chl.* under 660 nm laser irradiation in vitro

The existing research indicates that the cell components of *Chl.* contain abundant immune-stimulating substances [39], such as CWST, ARS-2, which can act as adjuvants and increase the activating of DCs and macrophages through toll-like receptors (TLR), such as TLR2. More importantly, intact *Chl.* had a very low activation level on bone marrow-derived dendritic cells (BMDCs) and RAW 264.7 cells (Figure S5a-c, S6a-c), immune-stimulating substances need to be released by *Chl.* to activate immune cells. *Chl.* can produce ROS apart from oxygen under excessive light irradiation, which can damage the center of photosystem (PS) and cause PSMs to die. Therefore, to verify the potential adjuvants releasing effect of *Chl.* under 660 nm laser *in vitro*, we first investigated the adjuvants released from *Chl.* post being treated by 660 nm laser (Fig. 3a). We found that *Chl.* will release a series of adjuvants. And we used high performance liquid chromatography-mass spectrometry (LC-MS) and spectrophotometry to detect and identify the supernatant ingredients, and we found that *Chl.* will release series water-soluble protein, glycoprotein, cholesterol, DNA and RNA (Fig. 3b). Meanwhile, the content of ARS-2, an identified adjuvant, increased significantly in the supernatant post PDT (Figure S4a-b). All of these ingredients will act as adjuvants by acting on multiple pattern recognition receptors on DCs or macrophages (such as TLR2, TLR9 and etc.). At the same time, DCs or macrophages will release a series of cytokines (IL-12 and etc.) and activate the adaptive immune response and tumor growth will be inhibited.

To test the adjuvants released under 660 nm laser can effectively activate APCs, we investigated the effect of *Chl.* supernatant post treated by 660 nm laser on BMDCs. *Chl.* supernatant post treated by 660 nm laser were mixed with BMDCs. Then the co-stimulatory molecules CD80 and CD86, which are well-known marker for BMDCs maturation were analyzed [45,46]. Results indicated that *Chl.* supernatant could enhance the activation of BMDCs, even higher than that of lipopolysaccharide (LPS) (Fig. 3c, Figure S5a, S5d). Activated DCs would secrete various types of cytokines to regulate other types of immune cells [47]. Thus, we used an ELISA kit to detect the amount of IL-12p70 and TNF- $\alpha$  in the supernatant of BMDCs after activation. Results indicated that both IL-12p70 and TNF- $\alpha$  were increased (Fig. 3d-e, Figure S5b-c, S5e-f),

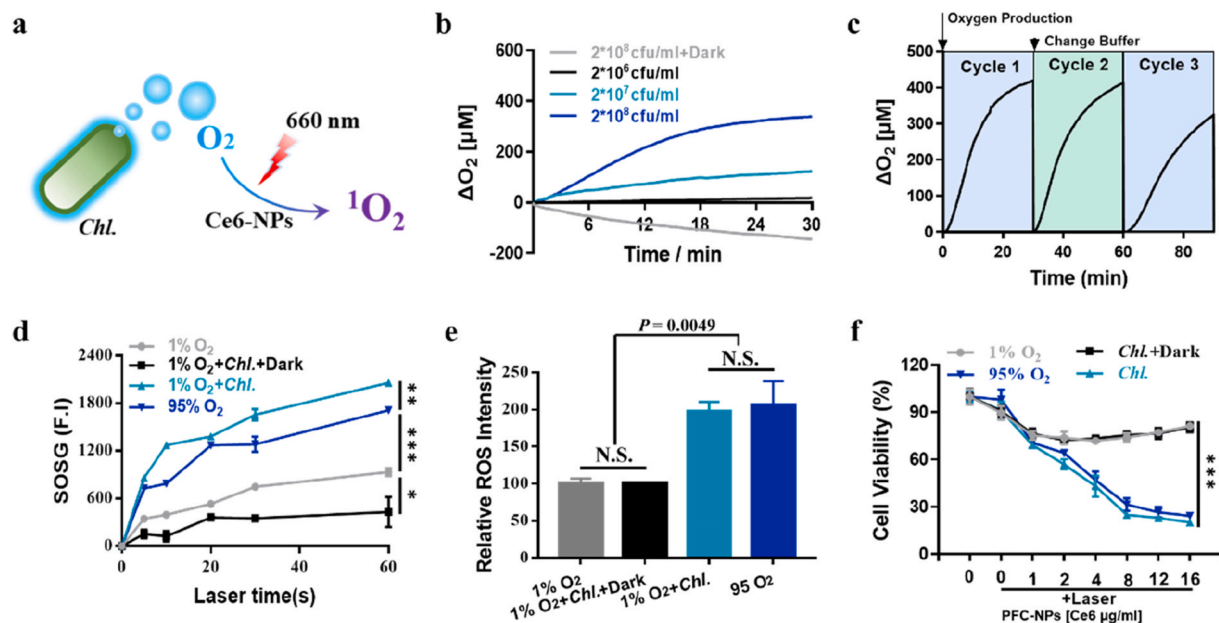


**Fig. 2.** Utilizing *Chl.* to enhance PDT based tumor cell killing *in vitro*. **a**, Schematic diagram of *Chl.* coupled PDT for enhanced local effect *in vitro*. **b**, O<sub>2</sub> production of different amount of *Chl.* under light irradiation. **c**, Repetitive O<sub>2</sub> production of *Chl.* under light irradiation. **d**, Quantification of  $^1O_2$  of Ce6-NPs under 660 nm laser irradiation determined by SOSG. **e**, Quantification of the relative ROS intensity of CT26 cells. **f**, Cytotoxicity of CT26 cells treated with varied concentrations of Ce6-NPs under 660 nm laser exposure measured by CCK-8 viability reagent. Data are representative or pooled and are expressed as Mean  $\pm$  SE. Asterisks indicate statistically significant differences as analyzed by One-Way ANOVA (\*\*\*  $p < 0.001$ , \*\*  $p < 0.01$ , \*  $p < 0.05$ , N.S.  $p > 0.05$ ).

indicating that *Chl.* supernatant could promote tumor antigens (TAs) to activate DC cells and thereby increase cellular immunity *in vitro*. Furthermore, we found that the results obtained on RAW264.7 cells can also indicate the *Chl.* post treated by 660 nm laser can promote M1 type macrophage polarization (Figure S3f-h, Figure S6), which will effectively reverse the immunosuppressive microenvironment within tumors. Hence, *Chl.* has very low immunogenicity, but it will release a series of immune activating substances to produce an adjuvant effect under 660 nm laser irradiation.

### 3.3. Enhanced anti-tumor local and abscopal effect of *Chl.* coupled PDT *in vivo*

To test the enhanced PDT effect on local tumor, we studied the anti-tumor effect of the *Chl.* coupled PDT on CT26 colon cancer model (Fig. 4a). To extend the survival time of *Chl.* in tumors, we mixed *Chl.* with sodium alginate solution for intra-tumoral injection. The results show that *Chl.* can still produce oxygen with a very efficient manner and effectively reverse tumor hypoxia (Figure S7). Following that, the tumor-bearing mice were divided into two groups, which were given Ce6-NPs + 660 nm or Ce6-NPs + *Chl.* + ~600 nm + 660 nm (*Chl.* coupled PDT). We found that Ce6-NPs accumulated at a maximum amount in tumor around 8 h after intravenous injection (Figure S8). The tumor inhibition rate of *Chl.* coupled PDT group reached nearly 75% compared with Ce6-NPs + 660 nm group (Fig. 4b, k, 4 m), and was significantly different from the other and body weight of each group of mice did not change significantly (Figure S12a). More importantly, in the *Chl.* coupled PDT group, more than 62.5% tumor-bearing mice can be completely cured (Fig. 4c). These experiments showed that *Chl.* coupled PDT has a significant inhibition effect on local tumors.

Simultaneously, we conducted the next experiment to determine whether *Chl.* coupled PDT would achieve effective anti-tumor immune effects in a dual tumor model (Fig. 4a). We found that *Chl.* coupled PDT did activate immune response against tumors after local tumor treatments (Figure S9, S10). We inoculated balb/c mice subcutaneously with different amount of CT26 cells on both the right (local tumor) and left (distal tumor) flanks 6 days before the treatment, respectively. On day 0,

the local tumors in all animals received laser irradiation, whereas the distal tumors were left untreated to assess the impact of systemic anti-tumor immunity. Results showed that the distal tumors were effectively suppressed at a tumor inhibition rate of 75% with a complete response rate of 50% in the *Chl.* coupled PDT group (Fig. 4d and e, 4k, 4 m). Meanwhile, flow cytometry analysis of the distal tumors showed an increased CD8<sup>+</sup> T cell infiltration on balb/c mice in the *Chl.* coupled PDT group than in simple PDT group (Figure 4n). And the immune cell activation was not triggered by the components of Ce6-NPs (Figure S11). To confirm that *Chl.* coupled PDT can directly act on local human tumors and the improved anti-tumor treatment effect of distal tumors is due to the systemic anti-tumor immune response, we introduced a nude mouse model (balb/c-nu mice) with human tumor cells A549 (Fig. 4f). The local tumors were effectively suppressed at a tumor inhibition rate of 65% with a complete response rate of 40% and the distal tumors inhibition was basically invalid at a tumor inhibition rate around 17% with no tumor exemption in the *Chl.* coupled PDT group (Fig. 4g-j, 4l-m). Body weight of each group of mice did not change significantly throughout the treatment period (Figure S12b).

### 3.4. Challenged tumor inhibition and enhanced anti-tumor immune memory via activating of *Chl.* coupled PDT *in vivo*

To prove that *Chl.* coupled PDT can enhance therapeutic effect on tumors that are more hypoxic, more immunosuppressive and more metastatic. We next studied the anti-tumor effect of the *Chl.* coupled PDT on hypoxic 4T1 breast cancer model (Fig. 5a). The tumor-bearing mice were divided into 6 groups, which were given normal saline, Ce6-NPs, *Chl.* + 660 nm, Ce6-NPs + 660 nm, Ce6-NPs + *Chl.* + 660 nm, Ce6-NPs + *Chl.* + ~600 nm + 660 nm (*Chl.* coupled PDT group). The tumor inhibition rate of *Chl.* coupled PDT group reached nearly 90% (Fig. 5b, Figure S13a, S13e), and was significantly different from others ( $p < 0.001$ ) and body weight of each group of mice did not change significantly (Figure S13b). More importantly, in the *Chl.* coupled PDT group, more than 54.5% tumor-bearing mice can be completely cured (Fig. 5c). These experiments showed that *Chl.* coupled PDT has a significant inhibition effect on local tumors.

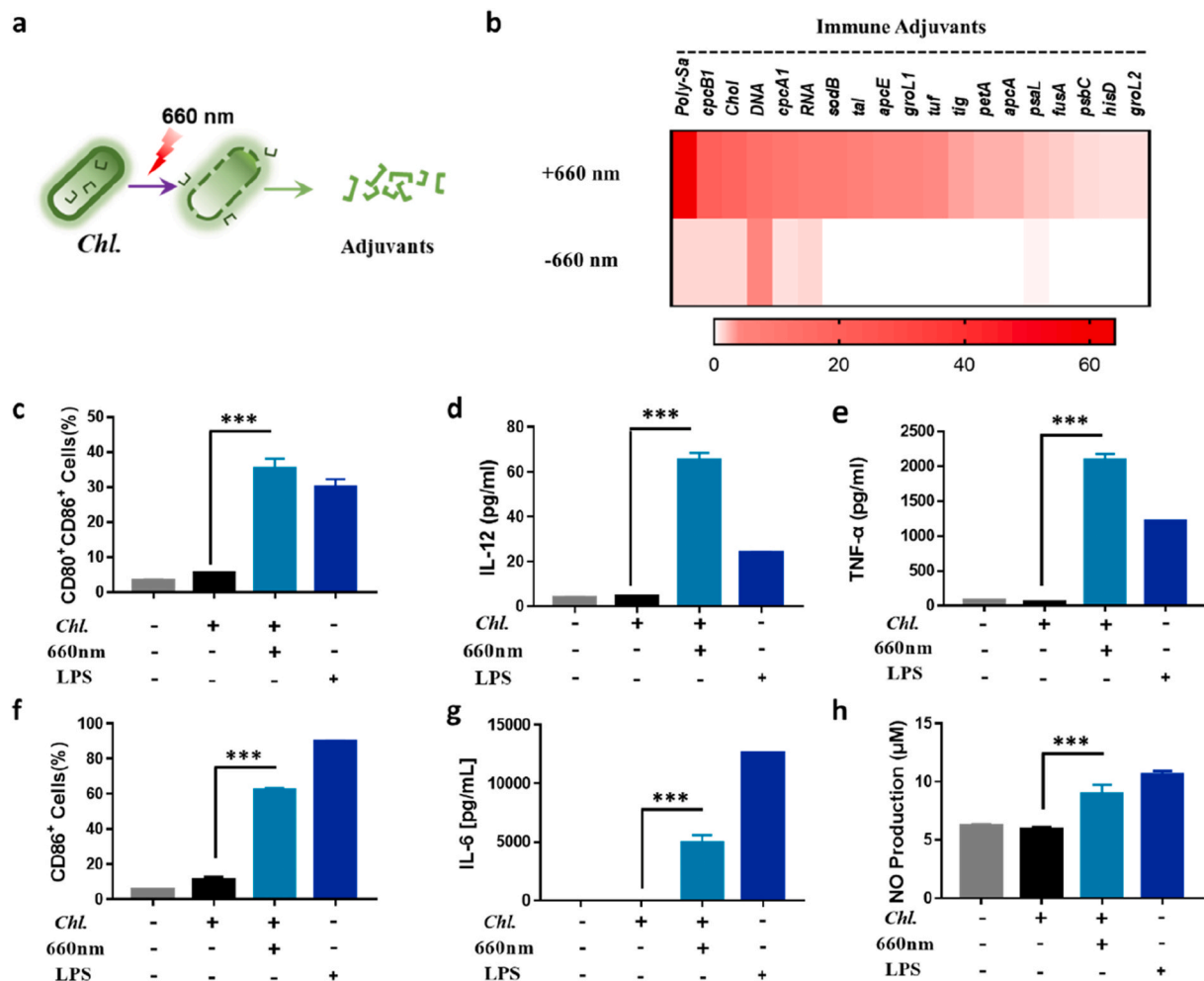


**Fig. 3.** Adjuvants released by *Chl.* under 660 nm laser irradiation *in vitro*. **a**, Schematic of adjuvants releasing of the *Chl.* by 660 nm laser irradiation. **b**, Mass spectrometry and spectrophotometry analysis of the relative abundance of polysaccharides (Poly-Sa), cholesterol (Chol), protein, DNA and RNA w/and w/o 660 nm laser irradiation. **c**, Quantification of the CD11c<sup>+</sup>CD80<sup>+</sup>CD86<sup>+</sup> BMDCs of the flow cytometry analysis post different treatments. **d**, IL-12p70 levels in supernatant of the BMDCs medium post different treatments. **e**, TNF-α levels in supernatant of the BMDCs medium post different treatments. **f**, Quantification of the CD45<sup>+</sup>F4/80<sup>+</sup>CD11b<sup>+</sup> CD86<sup>+</sup> RAW 264.7 of the flow cytometry analysis post different treatments. **g**, IL-6 levels in supernatant of the RAW 264.7 medium post different treatments. **h**, NO concentration in supernatant of the RAW 264.7 medium post different treatments. Each experimental group included  $n \geq 3$ . Data are representative or pooled and are expressed as Mean  $\pm$  SE. Asterisks indicate statistically significant differences as analyzed by One-Way ANOVA ( $*** p < 0.001$ ).

Afterwards, we designed experiments to prove that *Chl.* coupled PDT can indeed enhance the occurrence of anti-tumor immune response and strengthen the immune memory effect *in vivo*. And after we treated the local 4T1 tumor, we incubated 4T1 tumor (challenged tumor) again on the other side of mice post different treatments on the 19th day and detected the growth of the newly incubated tumors (Fig. 5a). The challenged tumors in the *Chl.* coupled PDT group were significantly suppressed, and the complete response rate of challenged tumors in the *Chl.* coupled PDT group reached 90.0% compared to 27.3% in the simple PDT group (Fig. 5d–e, Figure S13f). At the same time, we analyzed the  $T_{em}$  cells (CD44<sup>hi</sup> CD62L<sup>low</sup>, effector memory T cells) in spleen on the 19th day by flow cytometry, results showed an increased  $T_{em}$  amount, which revealed a stronger immune memory effect occurred (Fig. 5g, Figure S13c–d). More importantly, we removed the spleen at 29 d post the treatments, then isolated the white-blood cells in the spleen and co-incubated with 4T1 tumor cells (and its antigens), and finally detected the concentration of lactate dehydrogenase (LDH) and IFN-γ in the supernatant. The results showed that the cells in the spleen of the *Chl.* coupled PDT group can generate specific anti-tumor immune memory and specific anti-tumor immune response (Fig. 5h and i). All the results indicated that *Chl.* coupled PDT could notably enhance the anti-tumor immune effect and anti-tumor memory efficacy.

### 3.5. Enhanced anti-tumor metastasis effect by *Chl.* coupled PDT *in vivo*

Enhanced anti-tumor immune response can also reduce the incidence of metastatic tumors [48,49]. Primary tumors were removed via surgery at 14 days after treatment, the metastatic lesions were evaluated (Fig. 6a). The body weights decreased obviously in all other groups except the *Chl.* coupled PDT group from day 15–70, more than half of the mice lost more than 20% of their body weight especially in the simple PDT group (Figure S14). This might be the reason that the metastasized tumors affected normal tissues and organs. As we have imagined, *Chl.* coupled PDT could indeed be very effective in reducing lung metastases, while there are a large number of lung metastases in other groups, especially in simple PDT group (Fig. 6b–c, Figure S15). Panoramic scanning results of H&E sections showed that large areas of metastatic lesions with a condensed nucleus distinct from normal tissues were distributed in the lungs of all groups except *Chl.* coupled PDT group (Fig. 6b, Figure S15). The liver is another organ that is prone to tumor metastasis and we characterized the liver for metastases. Similar to the case of lung metastasis, the number of liver metastases were significantly inhibited in *Chl.* coupled PDT group compared to the other groups (Fig. 6b and d, Figure S15). Overall, this *Chl.* coupled PDT strategy can indeed enhance the anti-tumor immune response, and can indeed reduce

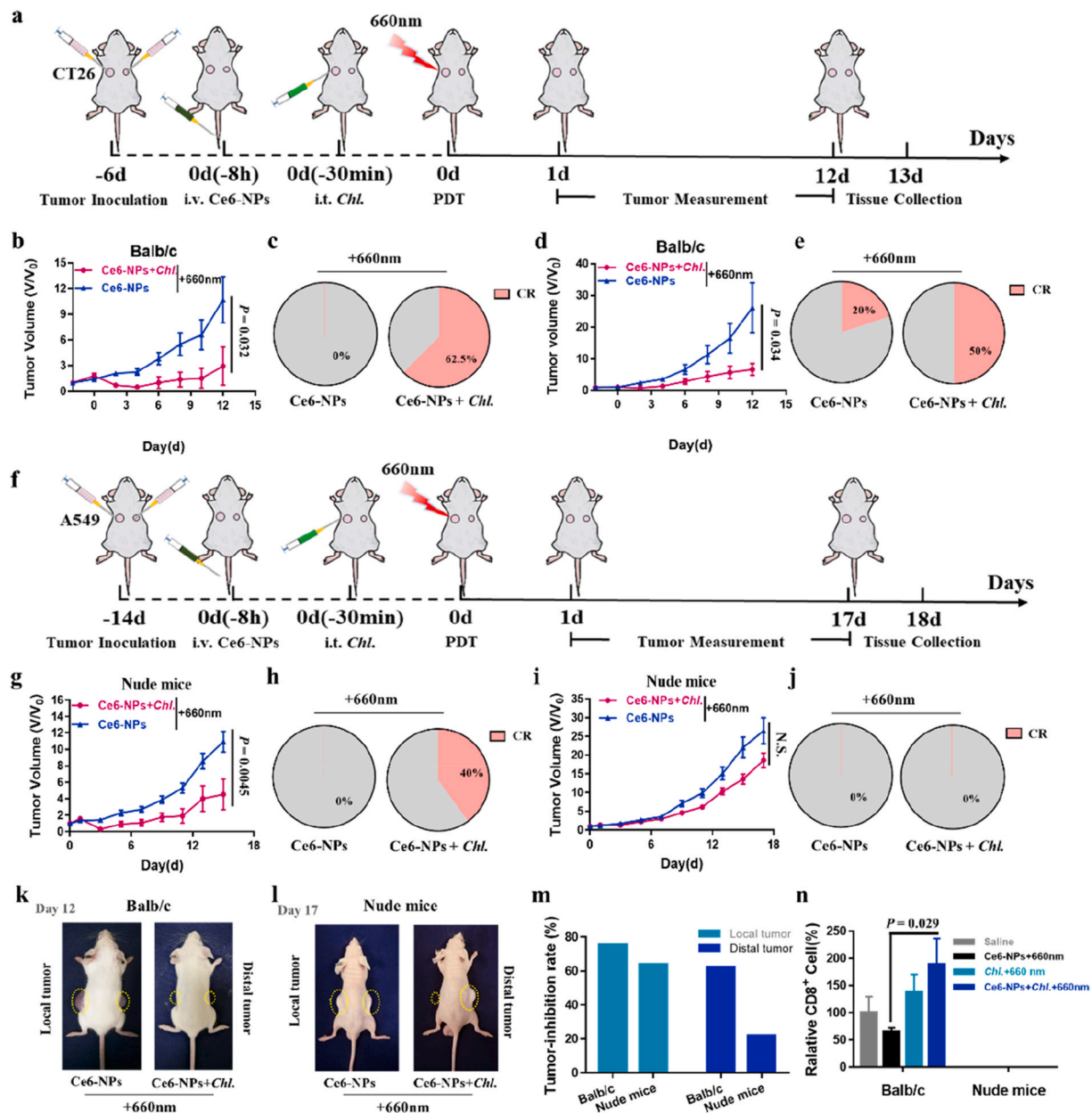


**Fig. 4.** Enhanced anti-tumor abscopal effect of *Chl.* coupled PDT *in vivo*. **a**, Experimental design to evaluate the abscopal effect on Balb/c mice (CT26 tumor cells). **b**, Tumor volume of the local tumors on Balb/c mice post various treatments. **c**, Local tumor complete responses rate on Balb/c mice post different treatments (CR: complete responses). **d**, Tumor volume of the distal tumors on Balb/c mice post various treatments. **e**, Distal tumor complete responses rate on Balb/c mice post different treatments (CR: complete responses). **f**, Experimental design to evaluate the nonexistent abscopal effect on nude mice (A549 tumor cells). **g**, Tumor volume of the local tumors on nude mice post various treatments. **h**, Local tumor complete responses rate on nude mice post different treatments (CR: complete responses). **i**, Tumor volume of the distal tumors on nude mice post various treatments. **j**, Distal tumor complete responses rate on nude mice post different treatments (CR: complete responses). **k**, Photographs of the balb/c mice at Day 12 post different treatments. **l**, Photographs of the nude mice at Day 17 post different treatments. **m**, Tumor inhibition rate of local and distal tumor on Balb/c and nude mice. **n**, Flow cytometry analysis quantification of the CD8<sup>+</sup> T cells in distal tumor post the four treatments (gated on CD3<sup>+</sup> cells). Each experimental group included  $n \geq 3$ . Data are representative or pooled and are expressed as Mean  $\pm$  SE. Asterisks indicate statistically significant differences as analyzed by One-Way ANOVA (N.S.  $p > 0.05$ ).

tumor metastases. It is worth noting that, at the dose we studied, *Chl.* coupled PDT showed a good killing efficiency, bio-compatibility and biosafety.

#### 4. Discussion and conclusion

Existing studies have shown that PDT can cause tumor cells to produce immunogenic cell death (ICD), which in turn leads to the production of adaptive anti-tumor immunity, but this circumstance is rare in clinical practice. Tumor will form a continuous hypoxic

microenvironment, and will release a series of immunosuppressive cytokines, such as interleukin 10 (IL-10) and tumor growth factor  $\beta$  (TGF- $\beta$ ) after PDT. Eventually, a severe immunosuppressive microenvironment within the tumor will be formed, which will eventually increase the probability of tumor recurrence and metastasis. In other words, PDT alone cannot induce an effective immune response. Existing research mainly focus on wrapping adjuvants in nanoparticles for tumor delivery, and this design has produced better therapeutic effects. *Chlorella* has a variety of immune adjuvants, which can activate APCs. Therefore, we studied the activation of *Chlorella* on immune response. *In vitro*

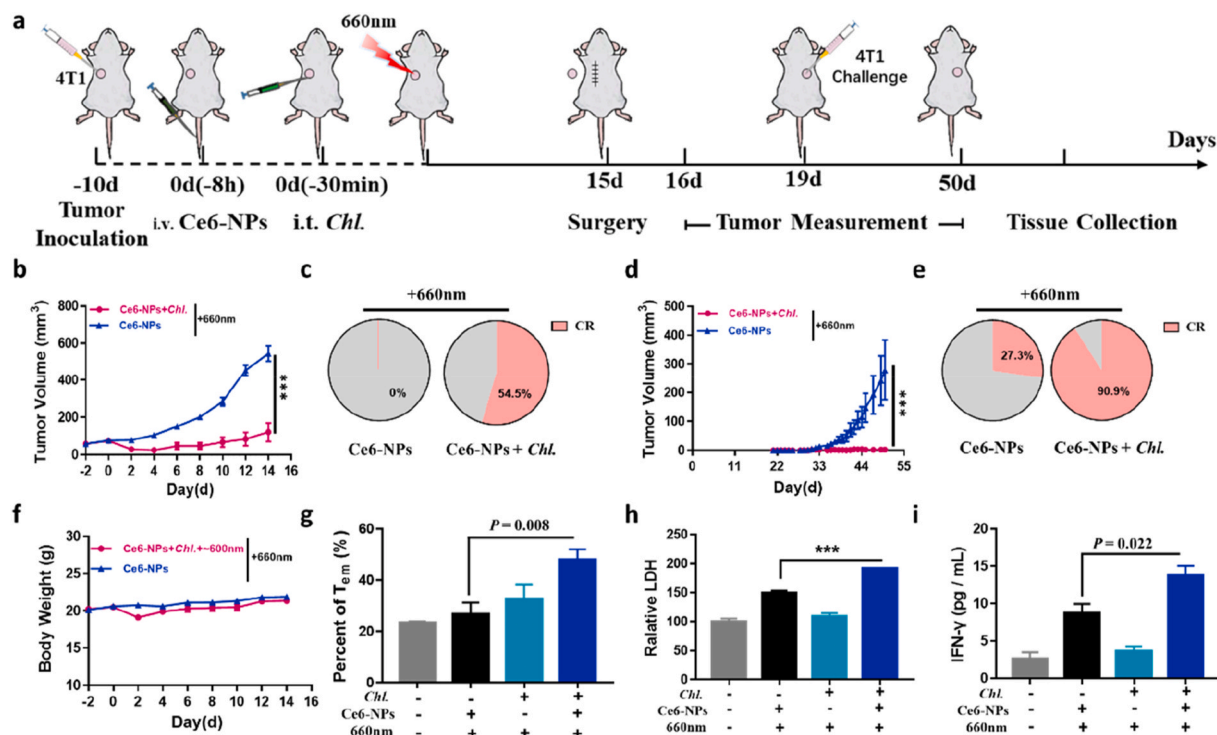


**Fig. 5.** Challenged tumor inhibition and enhanced anti-tumor immune memory via activating of *Chl.* coupled PDT *in vivo*. **a**, Experimental design to evaluate the tumor re-challenge inhibition and anti-tumor immune memory effect on Balb/c mice (4T1 tumor cells). **b**, Tumor volume of the local 4T1 tumors post various treatments. **c**, Local tumor complete responses rate post different treatments (CR: complete responses). **d**, Re-challenged tumor volume of the 4T1 tumors post various treatments after tumor challenge. **e**, Re-challenged tumor complete responses rate post different treatments (CR: complete responses). **f**, Body weight of the mice post various treatments. **g**, Flow cytometry analysis quantification of the CD44<sup>hi</sup>CD62L<sup>low</sup> T<sub>em</sub> cells in spleen post the four treatments (gated on CD3<sup>+</sup>CD8<sup>+</sup> cells). **h**, Relative LDH in the supernatant after co-incubation of spleen cells and 4T1 tumor cells. **i**, IFN- $\gamma$  concentration in the supernatant after co-incubation of spleen cells and 4T1 tumor antigen. Each experimental group included  $n \geq 3$ . Data are representative or pooled and are expressed as Mean  $\pm$  SE. Asterisks indicate statistically significant differences as analyzed by One-Way ANOVA (\*\*\*)  $p < 0.001$ .

experiments have shown that *Chlorella* after PDT can activate antigen-presenting cells and increase the release of inflammatory cytokines, such as IL-12p70 and TNF- $\alpha$ . At the same time, *Chlorella* alone can not produce a specific immune response to inhibit tumor growth. Therefore, *Chlorella* alone cannot activate the immune response. Yet they can be used directly as a very convenient synergist for the synergism of PDT. Therefore, the combination of the ability of photosynthetic microorganisms to produce oxygen and the ability to release adjuvants with PDT can strengthen PDT efficiency, reverse the tumor immunosuppressive microenvironment to a higher degree, enhance immune cells activation and ultimately reduce tumor recurrence and metastasis.

*Chl.* coupled PDT strategy we report here is a way to use the dual effect of *Chl.* to enhance PDT effect, including oxygen production and adjuvants release. Firstly, *Chl.* is a photosynthetic heterotrophic prokaryote that can produce large amounts of oxygen under light conditions, even more than 300  $\mu$ M in 30 min. Therefore, it can be used as a biological oxygen supplier to continuously deliver oxygen. This long-term oxygen supply can reverse the hypoxia of tumor tissues, enhance the effect of PDT, and can also reverse the further hypoxia that may occur after photodynamic therapy. Moreover, a controllable and efficient means of oxygen production is very promising for synergistic photodynamic therapy. Secondly, *Chl.* has low immunogenicity, but it contains a lot of immune activating substances, such as ARS-2 and etc., which can activate APCs through TLR2 and etc. These immune activating substances need to be controlled release before they can play a role in immune activation, and PDT is an effective means to promote the release of adjuvants by *Chlorella*. *Chl.* after PDT can produce more than 7 times the activation efficiency on antigen presenting cells (APCs), and increase the release of cytokines by more than 12 times, the activation level can even exceed LPS (10  $\mu$ g/ml). Therefore, the use of PDT here can

promote the release of immune adjuvants and activate anti-tumor adaptive immunity, which is worth looking forward to.

Here we combined the two characteristics of *Chl.* with PDT, and we find that the integration of *Chlorella* with PDT can significantly strengthen local tumor killing efficiency, enhance the specific anti-tumor immune response, and obtain powerful anti-tumor immune memory effect. The integration of *Chlorella* with PDT can inhibit the local tumor (tumor inhibition rate: 90%), as well as tumor recurrence (tumor inhibition rate: 100%) and tumor metastasis (tumor inhibition rate: 90%). And this process is produced by its own adaptive anti-tumor immune response. More importantly, *Chl.* coupled PDT can directly kill abscopal tumors (tumor inhibition rate: 75%). This process also greatly deepens the possibility of conversion of *Chl.* coupled PDT to treat the disseminated and undetectable tumors. This strategy can definitely improve the local and abscopal treatment effects of PDT on mice, and we also hope to adapt integration of *Chlorella* with PDT to large animals in future work to obtain effective immune response enhancement.

In conclusion, a *Chl.* coupled PDT strategy is developed that utilizing the dual effects of *Chl.* to produce oxygen for enhanced local tumor killing and release adjuvants for further immune activating under light irradiation simultaneously. Primary hypoxic tumor can be efficiently treated due to that *Chl.* coupled PDT can produce enough oxygen and generate sufficient <sup>1</sup>O<sub>2</sub> during laser-triggered PDT, thus producing enhanced TAAs. In addition, *Chl.* coupled PDT can release adjuvants and activate APCs and etc. within immunosuppressed tumors, and produce effective anti-tumor immune response. Ultimately, *Chl.* coupled PDT reduces the incidence of tumor metastases and tumor recurrence after PDT. On the whole, this *Chl.* coupled PDT strategy generates enhanced local tumor killing, boosts anti-tumor immune responses and promotes immune memory effect, which may be a great progress for realizing

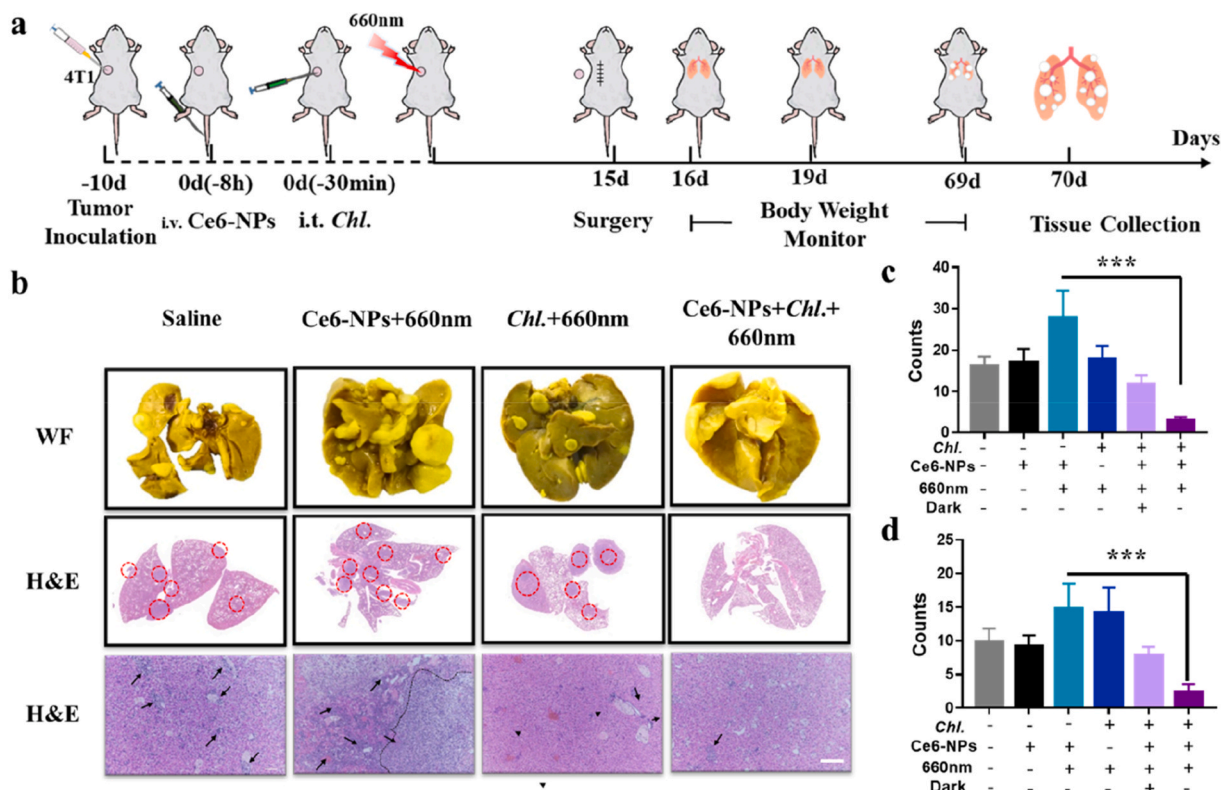


**Fig. 6.** Enhanced anti-tumor metastasis effect of *Chl.* coupled PDT *in vivo*. **a**, Experimental design to evaluate the anti-tumor metastasis effect on Balb/c mice (4T1 tumor cells). **b**, Photographs following WF are the white filed images of lung tissues after staining with Bouin's Fluid. Photographs in the middle are the panoramic scanning photographs of the H&E staining of lung tissues. Photographs below are the images of the H&E staining of liver tissues. (Scale bar = 100  $\mu$ m) **c**, Quantification of metastatic lesions of the lung tissues. **d**, Quantification of metastatic lesions of the liver tissues. Each experimental group included  $n \geq 3$ . Data are representative or pooled and are expressed as Mean  $\pm$  SE. Asterisks indicate statistically significant differences as analyzed by One-Way ANOVA (\*\*\*)  $p < 0.001$ .

systemic effect of PDT.

#### CRediT authorship contribution statement

**Haoran Wang:** Conceptualization, Methodology, Investigation, Visualization, Writing – original draft, Writing – review & editing. **Honghui Liu:** Investigation. **Yunfei Guo:** Investigation. **Wenjing Zai:** Investigation. **Xianghui Li:** Investigation, during revise. **Wei Xiong:** Investigation. **Xiaozhi Zhao:** Investigation, Writing – review & editing. **Yingfang Yao:** Review during revise. **Yiqiao Hu:** Supervision, Writing – review & editing, Funding acquisition. **Zhigang Zou:** Supervision, Writing – review & editing. **Jinhui Wu:** Conceptualization, Supervision, Writing – review & editing, Funding acquisition.

#### Declaration of competing interest

The authors declare that they have no known competing financial interests or personal relationships that could have appeared to influence the work reported in this paper.

#### Acknowledgments

This paper was supported by National Key R&D Program of China (2017YFA0205400); National Natural Science Foundation of China (No. 31872755, 81872811, 32171372); Jiangsu Outstanding Youth Funding (BK20190007); This project was also supported by the Central Fundamental Research Funds for the Central Universities (02141438473).

#### Appendix A. Supplementary data

Supplementary data related to this article can be found at <https://doi.org/10.1016/j.bioactmat.2021.10.028>.

[.org/10.1016/j.bioactmat.2021.10.028](https://doi.org/10.1016/j.bioactmat.2021.10.028).

#### References

- [1] W.H. Fridman, et al., The immune contexture in cancer prognosis and treatment, *Nat. Rev. Clin. Oncol.* 14 (12) (2017) 717–734.
- [2] J. Nam, et al., Chemo-photothermal therapy combination elicits anti-tumor immunity against advanced metastatic cancer, *Nat. Commun.* 9 (1) (2018) 1074.
- [3] F. Zhou, et al., Tumor microenvironment-activatable prodrug vesicles for nanoenabled cancer chemoimmunotherapy combining immunogenic cell death induction and CD47 blockade, *Adv. Mater.* 31 (14) (2019), e1805888.
- [4] X. Li, et al., Innovative strategies for hypoxic-tumor photodynamic therapy, *Angew Chem. Int. Ed. Engl.* 57 (36) (2018) 11522–11531.
- [5] L. Cheng, et al., Functional nanomaterials for phototherapies of cancer, *Chem. Rev.* 114 (21) (2014) 10869–10939.
- [6] C. Liang, et al., Emerging nanomedicine approaches fighting tumor metastasis: animal models, metastasis-targeted drug delivery, phototherapy, and immunotherapy, *Chem. Soc. Rev.* 45 (22) (2016) 6250–6269.
- [7] Z. Zhou, et al., Reactive oxygen species generating systems meeting challenges of photodynamic cancer therapy, *Chem. Soc. Rev.* 45 (23) (2016) 6597–6626.
- [8] S.H. Yun, S.J.J. Kwok, Light in diagnosis, therapy and surgery, *Nat Biomed Eng* 1 (2017).
- [9] X. Song, et al., Ultrasound triggered tumor oxygenation with oxygen-shuttle nanoporphyrin to overcome hypoxia-associated resistance in cancer therapies, *Nano Lett.* 16 (10) (2016) 6145–6153.
- [10] M.W. Dewhirst, Y. Cao, B. Moeller, Cycling hypoxia and free radicals regulate angiogenesis and radiotherapy response, *Nat. Rev. Cancer* 8 (2008) 425.
- [11] V.P. Chauhan, et al., Angiotensin inhibition enhances drug delivery and potentiates chemotherapy by decompressing tumour blood vessels, *Nat. Commun.* 4 (2013) 2516.
- [12] Y. Cheng, et al., Perfluorocarbon nanoparticles enhance reactive oxygen levels and tumour growth inhibition in photodynamic therapy, *Nat. Commun.* 6 (2015) 8785.
- [13] H. Ren, et al., Relighting photosensitizers by synergistic integration of albumin and perfluorocarbon for enhanced photodynamic therapy, *ACS Appl. Mater. Interfaces* 9 (4) (2017) 3463–3473.
- [14] M. Gao, et al., Erythrocyte-Membrane-enveloped perfluorocarbon as nanoscale Artificial red blood cells to relieve tumor hypoxia and enhance cancer radiotherapy, *Adv. Mater.* 29 (35) (2017), 1701429.

- [15] Y. Zhang, et al., Pd@Au bimetallic nanoplates decorated mesoporous MnO<sub>2</sub> for synergistic nucleus-targeted NIR-II photothermal and hypoxia-relieved photodynamic therapy, *Adv Healthc Mater* 9 (2) (2020), e1901528.
- [16] W.T. Zhang, et al., Oxygen-Generating MnO<sub>2</sub> nanodots-anchored versatile nanoplateform for coupled chemo-photodynamic therapy in hypoxic cancer, *Adv. Funct. Mater.* 28 (13) (2018).
- [17] W.W. Zhu, et al., Modulation of hypoxia in solid tumor microenvironment with MnO<sub>2</sub> nanoparticles to enhance photodynamic therapy, *Adv. Funct. Mater.* 26 (30) (2016) 5490–5498.
- [18] Y.T. Fan, et al., Modulation of intracellular oxygen pressure by dual-drug nanoparticles to enhance photodynamic therapy, *Adv. Funct. Mater.* 29 (10) (2019).
- [19] D.R. Hu, et al., Perfluorocarbon-loaded and redox-activatable photosensitizing agent with oxygen supply for enhancement of fluorescence/photoacoustic imaging guided tumor photodynamic therapy, *Adv. Funct. Mater.* 29 (9) (2019).
- [20] L. Galluzzi, et al., Immunogenic cell death in cancer and infectious disease, *Nat. Rev. Immunol.* 17 (2) (2017) 97–111.
- [21] C. He, et al., Core-shell nanoscale coordination polymers combine chemotherapy and photodynamic therapy to potentiate checkpoint blockade cancer immunotherapy, *Nat. Commun.* 7 (2016) 12499.
- [22] M.J. Schuijs, H. Hammad, B.N. Lambrecht, Professional and 'amateur' antigen-presenting cells in type 2 immunity, *Trends Immunol.* 40 (1) (2019) 22–34.
- [23] P. Michea, et al., Adjustment of dendritic cells to the breast-cancer microenvironment is subset specific, *Nat. Immunol.* 19 (8) (2018) 885–897.
- [24] W. Song, et al., Enhanced immunotherapy based on photodynamic therapy for both primary and lung metastasis tumor eradication, *ACS Nano* 12 (2) (2018) 1978–1989.
- [25] S.J. Gan, et al., Covalent organic framework-supported molecularly dispersed near-infrared dyes boost immunogenic phototherapy against tumors, *Adv. Funct. Mater.* 29 (46) (2019).
- [26] F. Bonacina, et al., Myeloid apolipoprotein E controls dendritic cell antigen presentation and T cell activation, *Nat. Commun.* 9 (1) (2018) 3083.
- [27] R. Liang, et al., Oxygen-boosted immunogenic photodynamic therapy with gold nanocages@manganese dioxide to inhibit tumor growth and metastases, *Biomaterials* 177 (2018) 149–160.
- [28] B.Q. Spring, D. Kessel, 3D culture models of malignant mesothelioma reveal a powerful interplay between photodynamic therapy and kinase suppression offering hope to reduce tumor recurrence, *Photochem. Photobiol.* 95 (1) (2019) 462–463.
- [29] H. Wang, et al., Light-controlled oxygen production and collection for sustainable photodynamic therapy in tumor hypoxia, *Biomaterials* 269 (2020), 120621.
- [30] X. Yi, et al., Bacteria-triggered tumor-specific thrombosis to enable potent photothermal immunotherapy of cancer, *Science Advances* 6 (33) (2020), eaba3546.
- [31] H. Wang, et al., Photosynthetic microorganisms-based biophotothermal therapy with enhanced immune response, *Small* 17 (18) (2021), e2007734.
- [32] Y. Najm, S. Jeong, T. Leiknes, Nutrient utilization and oxygen production by *Chlorella vulgaris* in a hybrid membrane bioreactor and algal membrane photobioreactor system, *Bioresour. Technol.* 237 (2017) 64–71.
- [33] D.Y. Su, et al., Enzyme-modulated anaerobic encapsulation of *Chlorella* cells allows switching from O<sub>2</sub> to H<sub>2</sub> production, *Angew. Chem. Int. Ed.* 58 (12) (2019) 3992–3995.
- [34] C.S. Jones, S.P. Mayfield, Algae biofuels: versatility for the future of bioenergy, *Curr. Opin. Biotechnol.* 23 (3) (2012) 346–351.
- [35] H.Y. Hsu, et al., Immunostimulatory bioactivity of algal polysaccharides from *Chlorella pyrenoidosa* activates macrophages via Toll-like receptor 4, *J. Agric. Food Chem.* 58 (2) (2010) 927–936.
- [36] N.T. Chou, et al., *Chlorella sorokiniana*-induced activation and maturation of human monocyte-derived dendritic cells through NF- $\kappa$ B and PI3K/MAPK pathways, *Evid Based Complement Alternat Med* 2012 (2012), 735396.
- [37] K. Tanaka, et al., Oral administration of *Chlorella vulgaris* augments concomitant antitumor immunity, *Immunopharmacol. Immunotoxicol.* 12 (2) (1990) 277–291.
- [38] E.S. Bergmann-Leitner, W.W. Leitner, Adjuvants in the driver's seat: how magnitude, type, fine specificity and longevity of immune responses are driven by distinct classes of immune potentiators, *Vaccines (Basel)* 2 (2) (2014) 252–296.
- [39] T. Hasegawa, et al., Toll-like receptor 2 is at least partly involved in the antitumor activity of glycoprotein from *Chlorella vulgaris*, *Int. Immunopharm.* 2 (4) (2002) 579–589.
- [40] H. Ren, et al., Oxygen self-enriched nanoparticles functionalized with erythrocyte membranes for long circulation and enhanced phototherapy, *Acta Biomater.* 59 (2017) 269–282.
- [41] Z.G. Zhou, et al., Perfluorocarbon nanoparticle-mediated platelet inhibition promotes intratumoral infiltration of T cells and boosts immunotherapy, *Proc. Natl. Acad. Sci. U.S.A.* 116 (24) (2019) 11972–11977.
- [42] W.G. Wang, et al., Perfluorocarbon regulates the intratumoural environment to enhance hypoxia-based agent efficacy, *Nat. Commun.* 10 (2019).
- [43] Z.G. Zhou, et al., Perfluorocarbon nanoparticles mediated platelet blocking disrupt vascular barriers to improve the efficacy of oxygen-sensitive antitumor drugs, *Small* 14 (45) (2018).
- [44] Z.G. Zhou, et al., Two-stage oxygen delivery for enhanced radiotherapy by perfluorocarbon nanoparticles, *Theranostics* 8 (18) (2018) 4898–4911.
- [45] K. Palucka, J. Banchereau, Cancer immunotherapy via dendritic cells, *Nat. Rev. Cancer* 12 (4) (2012) 265–277.
- [46] M. Colonna, G. Trinchieri, Y.J. Liu, Plasmacytoid dendritic cells in immunity, *Nat. Immunol.* 5 (12) (2004) 1219–1226.
- [47] T. Fukao, et al., PI3K-mediated negative feedback regulation of IL-12 production in DCs, *Nat. Immunol.* 3 (9) (2002) 875–881.
- [48] M. Chen, et al., Adrenergic stress constrains the development of anti-tumor immunity and abscopal responses following local radiation, *Nat. Commun.* 11 (1) (2020) 1821.
- [49] X. Han, et al., In situ thermal ablation of tumors in combination with nano-adjuvant and immune checkpoint blockade to inhibit cancer metastasis and recurrence, *Biomaterials* 224 (2019), 119490.